Rashba quantum wire: exact solution and ballistic transport

2007 J. Phys.: Condens. Matter 19 186227

(http://iopscience.iop.org/0953-8984/19/18/186227)

IOP PUBLISHING JOURNAL OF PHYSICS: CONDENSED MATTER

J. Phys.: Condens. Matter **19** (2007) 186227 (15pp) doi:10.1088/0953-8984/19/18/186227

Rashba quantum wire: exact solution and ballistic transport

C A Perroni[1], D Bercioux[2,3], V Marigliano Ramaglia[4] and V Cataudella[4]

[1] Institut für Festkörperforschung (IFF), Forschungszentrum Jülich, D-52425 Jülich, Germany
[2] Institut für Theoretische Physik, Universität Regensburg, D-93040 Regensburg, Germany
[3] Physikalisches Institut, Albert-Ludwigs-Universität, D-79104 Freiburg, Germany
[4] Coherentia-CNR-INFM and Dipartimento di Scienze Fisiche, Università degli Studi di Napoli 'Federico II', I-80126 Napoli, Italy

Received 16 November 2006, in final form 7 March 2007
Published 13 April 2007
Online at stacks.iop.org/JPhysCM/19/186227

Abstract

The effect of Rashba spin–orbit interaction in quantum wires with hard-wall boundaries is discussed. The exact wavefunction and eigenvalue equation are worked out, pointing out the mixing between the spin and spatial parts. The spectral properties are also studied within perturbation theory with respect to the strength of the spin–orbit interaction and diagonalization procedure. A comparison is made with the results of a simple model, the two-band model, that takes account only of the first two sub-bands of the wire. Finally, the transport properties within the ballistic regime are analytically calculated for the two-band model and through a tight-binding Green function for the entire system. Single and double interfaces separating regions with different strengths of spin–orbit interaction are analysed by injecting carriers into the first and the second sub-band. It is shown that in the case of a single interface the spin polarization in the Rashba region is different from zero, and in the case of two interfaces the spin polarization shows oscillations due to spin-selective bound states.

(Some figures in this article are in colour only in the electronic version)

1. Introduction

Spintronics [1] is one of the most prominent fields of modern condensed matter physics. Its target is to use spin to create electrical and optoelectronic devices with new functionalities [2]. Up to now, starting from the seminal device by Datta and Das [3], several devices based on giant and tunnel magnetoresistance have been realized for use as read-head sensors and magnetic random-access memories [2]. The important task of the integration of such spintronics technologies with classical semiconductor devices encounters an obstacle in the small spin injection from magnetic to semiconductor materials due to the large resistivity mismatch between magnetic and semiconductor materials [4]. For this reason it is useful to design

semiconductor devices with an efficient all-electrical spin injection and detection via Ohmic contacts at the Fermi energy, as has been already realized for metallic devices [5, 6].

Two important classes of spin–orbit interaction (SOI) are relevant for semiconductor spintronics: Dresselhaus-type coupling [7] and Rashba-type [8] coupling. The former arises from the lack of symmetry in the bulk inversion whereas the latter arises from the asymmetry along the growing-direction axis of the confining quantum well electric potential that creates a two-dimensional electron gas (2DEG) on a narrow-gap semiconductor surface. Since the Rashba SOI can be tuned by an external gate electrode [9–11] it is envisaged as a tool to control the precession of the electron spin in the Datta–Das proposal for a field-effect spin transistor [3].

Quasi-one-dimensional electron gases or quantum wires (QWs) are realized by applying split gates on top of a 2DEG in a semiconductor heterostructure [12]. The main effect owing to the confining potential is quantization of the electron motion in the direction orthogonal to the wire axis. The combination of this confining potential and the Rashba SOI gives rise to sub-band hybridization that can affect the working principle of the field-effect spin transistor. Mireles and Kirczenow [13] have numerically studied this effect and they have shown that a large value of the Rashba SOI can produce dramatic changes in the transport properties of the device and even suppress the expected spin modulation. The effect of sub-band hybridization has been investigated by Governale and Zülicke [14] in a QW with parabolic confinement. They show that electrons with large wavevectors in the lowest spin-split sub-bands have essentially parallel spin. But in proximity of the anti-crossing points due to the sub-band hybridization it is no longer appropriate to use the spin quantum number in order to characterize the electron state in the QW. Furthermore, they show that it is not possible to transfer the finite spin polarization of the QW to some external leads.

In this paper we study the spectral and the transport properties of a QW in the presence of SOI. The main result of this paper is to show how to achieve non-zero spin polarization in external leads using spin-unpolarized injected carriers. This can be obtained by injecting carriers in all the active sub-bands due to the quantum confinement. At the opening of each new sub-band the hybridization owing to SOI gives rise to spin-selective bound states reflecting in an oscillating spin polarization. Here, we want to stress that those spin-polarized bound states are not in contradiction with any fundamental symmetry property of the system [15].

This paper is organized in the following way. In section 2 we evaluate the spectral properties using the wavefunction approach [16–18]. In section 3 we provide an exact calculation for the spectral properties investigated within the perturbation theory approach and with exact diagonalization in a truncated Hilbert space. Here we also introduce a minimal model featuring the basic characteristic of a QW with SOI named the *two-band* model. This is used in section 4 in order to study the transport properties of a QW in the presence of a single interface between a region with and without SOI and in the case of a double interface (spin-field-effect transistor scheme). Our conclusions end the paper.

2. Exact solution of Rashba quantum wire: wavefunction

Let us consider a 2DEG filling the plane (x, z). The charge carriers have momentum $\vec{p} \equiv (p_x, p_z)$ and effective mass m. The particles are confined along the z-direction by the potential $V(z)$ and are subjected to the Rashba spin–orbit interaction (SOI). The single-particle Hamiltonian reads

$$\mathcal{H} = \frac{1}{2m}\left(p_x^2 + p_z^2\right) + V(z) + \mathcal{H}_{\mathrm{R}}, \tag{1}$$

where $\mathcal{H}_{\mathrm{R}}$ is the Rashba SOI

$$\mathcal{H}_{\mathrm{R}} = \frac{\hbar k_{\mathrm{SO}}}{m} (\sigma_z p_x - \sigma_x p_z) . \tag{2}$$

In equation (2), σ_x and σ_z are the x and z components, respectively, of the vector $\vec{\sigma}$ of Pauli matrices, and k_{SO} is the SOI constant. This can be tuned by means of external gates perpendicular to the 2DEG [9–11].

In the following we assume that the potential $V(z)$ provides a confinement with hard walls at $z = 0$ and W. The strategy to find the wavefunction of the Hamiltonian (1) is similar to the procedure followed in the absence of SOI: one exactly solves the 2D problem, then considers the quantizing effect of confinement on the wavefunction $\psi(x, z)$. In section 2.1 we briefly recall the spin-dependent solution of the 2DEG with SOI, then we impose the boundary conditions $\psi(x, z = 0) = \psi(x, z = W) = 0$. In the presence of SOI, these relations mix the z part of the wavefunction with its spinor component.

2.1. Solution without confinement

Without confinement both components of the momentum $\vec{p} = \hbar\vec{k}$ are conserved. The eigenfunctions of the Hamiltonian (1) in the absence of confining potential $V(z) = 0$ are denoted by the two spin modes $(+)$ and $(-)$, and read

$$\psi_{\vec{k},+}(x, z) = \exp\left[\mathrm{i}(k_x x + k_z z)\right] \begin{pmatrix} \cos(\theta/2) \\ -\sin(\theta/2) \end{pmatrix}, \tag{3a}$$

$$\psi_{\vec{k},-}(x, z) = \exp\left[\mathrm{i}(k_x x + k_z z)\right] \begin{pmatrix} \sin(\theta/2) \\ \cos(\theta/2) \end{pmatrix}, \tag{3b}$$

whose corresponding eigenvalues are given by

$$E_{\pm} = \frac{\hbar^2}{2m} \left(k^2 \pm 2k k_{\mathrm{SO}}\right), \tag{4}$$

where $k = \sqrt{k_x^2 + k_z^2}$ is the modulus of the wavevector in the x, z plane, $k_x = k\cos(\theta)$, $k_z = k\sin(\theta)$, with θ the angle formed between the vector $\vec{k}$ and the x axis. It is clear for equations (3*a*), (3*b*) that the spinors $\chi_{\pm}$ of the two modes are orthogonal to each other. We recall that the Rashba SOI can be viewed as a magnetic field parallel to the (x, z) plane and orthogonal to the wavevector $\vec{k}$. The net effect is to orientate the spin along the direction perpendicular to the wavevector [16].

In order to determine the solution with confinement, it is essential to find the eigenfunctions in the free case when the total energy E and the momentum along k_x are fixed (see figure 1). Fixing the total energy E, we note that there are two values of total momentum k, corresponding to the different modes, fulfilling equation (4) expressed as a linear combination of those four waves:

$$k_{\pm} = \sqrt{\frac{2m}{\hbar^2} E + k_{\mathrm{SO}}^2} \mp k_{\mathrm{SO}}. \tag{5}$$

The propagation directions for the $k_{\pm}$ modes are fixed by the momentum k_x. For $E > 0$, the mode $(+)$ is characterized by the propagation direction $\pm\alpha = \arccos(k_x/k_+)$ fixing the value of $k_z = \pm k_+ \sin(\alpha)$, whereas the mode $(-)$ has propagation direction $\pm\beta = \arccos(k_x/p_-)$ and $k_z = \pm k_- \sin(\beta)$. Therefore, the generic wavefunction $\psi_{E,k_x}(x, z)$ is given by

$$\psi_{E,k_x}(x, z) = \mathrm{e}^{\mathrm{i}k_x x} \left[A\psi_{1,E}^{(+)}(z) + B\psi_{2,E}^{(+)}(z) + C\psi_{1,E}^{(-)}(z) + D\psi_{2,E}^{(-)}(z)\right], \tag{6}$$

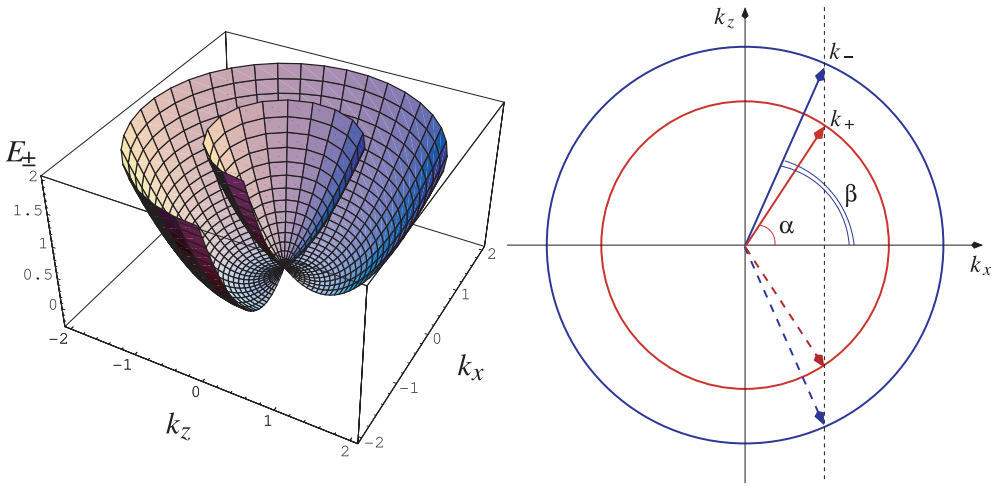

Figure 1. Left panel: spectrum of the two-dimensional electron gas in the presence of SOI interaction as a function of the wavevectors k_x and k_y. At fixed positive energy, the wavevectors of the mode (+) and (−) are on two concentric circles (radius for (−) mode larger than that for the (+) mode). Right panel: at fixed positive energy and x component of the wavevector, the four possible values of the z component are shown.

with

$$\psi^{(+)}_{\ell,E}(z) = \mathrm{e}^{-\mathrm{i}(-1)^{\ell}k_+ z\sin(\alpha)}\begin{pmatrix}\cos(\alpha/2)\\(-1)^{\ell}\sin(\alpha/2)\end{pmatrix}, \tag{7}$$

$$\psi^{(-)}_{\ell,E}(z) = \mathrm{e}^{-\mathrm{i}(-1)^{\ell}k_- z\sin(\beta)}\begin{pmatrix}-(-1)^{\ell}\sin(\beta/2)\\\cos(\beta/2)\end{pmatrix}, \tag{8}$$

and $\ell = 1, 2$.

For $-k_- \leqslant k_x < -k_+$ or $k_+ < k_x \leqslant k_-$, the wavefunction (6) is still valid. However, one has $\alpha = \mathrm{i}a$, implying that $\cos(\alpha) = \cosh(a)$ and $\sin(\alpha) = \mathrm{i}\sinh(a)$, therefore the (+) mode becomes an evanescent one. Moreover, if $k_x > k_-$ or $k_x < -k_-$, then $\beta = \mathrm{i}b$ and also the (−) mode changes into an evanescent one.

For $E < 0$ the four values of k_z are only relative to modes (−). A wavefunction similar to (6) can be written. Also in this case the Fermi surface is formed by two circles, but now they correspond to the same energy E_-. However, in the next section, we will see that, from weak to intermediate values of the Rashba SO coupling, only positive values of the energy are important due to the effect of the confinement.

2.2. Solution with confinement

The wavefunction (6) represents the starting point for taking account of the confinement. In fact, the hard-wall boundary conditions are obtained by imposing that the wavefunction is zero on the borders ($z = 0$ and W): $\psi_{E,k_x}(x, z = 0) = \psi_{E,k_x}(x, z = W) = 0$. For $E > 0$, we get the following exact eigenvalue equation for the Rashba quantum wire:

$$1 - \cos[k_+ W\sin(\alpha)]\cos[k_- W\sin(\beta)] + \sin[k_+ W\sin(\alpha)]\sin[k_- W\sin(\beta)]\frac{[1+\cos(\alpha)\cos(\beta)]}{\sin(\alpha)\sin(\beta)} = 0. \tag{9}$$

Therefore, via the SOI, the quantities k_+ and k_-, and clearly the energy, are related to the spinor components of the wavefunction. A similar equation is valid for $E < 0$.

In the absence of SOI, the quantized energy levels are independent of spin behaviour. Actually, one gets $k_\pm = \sqrt{2mE/\hbar^2}$ and $\alpha = \beta$. This yields

$$\sqrt{\frac{2mE}{\hbar^2}}\, W \sin(\alpha) = n\pi, \tag{10}$$

with n being a positive integer number, so that, together with the relation $\cos(\alpha) = k_x/k_\pm$, we obtain

$$E_n = \frac{\hbar^2}{2m}\left(\frac{n^2\pi^2}{W^2} + k_x^2\right), \tag{11}$$

which are the energy values for the sub-bands of the quantum wire without SOI.

In the presence of SOI, an important limit is obtained for $k_x = 0$. Indeed the eigenvalue equation becomes

$$\cos[(k_+ + k_-)W] = 1, \tag{12}$$

implying that

$$E_n = \frac{\hbar^2}{2m}\left(\frac{n^2\pi^2}{W^2} - k_{\mathrm{SO}}^2\right). \tag{13}$$

Therefore, all the sub-bands are shifted down by the SOI term k_{SO}^2. For values of the SOI such that $k_{\mathrm{SO}} < \pi/W$, the energies are positives and the wavefunction (6) holds true. This means that the spin-precession length $L_{\mathrm{SO}} = \pi/k_{\mathrm{SO}}$ has to be larger than the wire width.

3. Two-band model and perturbation theory

In the previous section we started from the wavefunction of the 2D model with SOI, and then imposed the conditions due to confinement. Now, we consider the opposite point of view. First we take into account the exact solution of the quantum wire in the absence of SOI, then we study its effect on the sub-bands. Because of SOI, a coupling between sub-bands with opposite spins occurs. In order to study the effects of this coupling, in section 3.1 we will discuss the results within the first- and second-order perturbation theory approach with respect to the SOI. In section 3.2 we consider the two-band model, where only the first two bands of the unperturbed spectrum are assumed to be coupled by the interaction. This assumption is valid if the wire is very narrow. Moreover, this simple system is studied since it provides a simple understanding of the transport properties. Finally, in section 3.3, we will show the results of the exact diagonalization of the model.

The Hamiltonian (1) is considered to be split into two terms: $\mathcal{H}_0$ and $\mathcal{H}_{\mathrm{R}}$. The term $\mathcal{H}_0$ is simply the Hamiltonian of the wire without SOI:

$$\mathcal{H}_0 = \frac{1}{2m}\left(p_x^2 + p_z^2\right) + V(z), \tag{14}$$

where $V(z)$ is the hard-wall confining potential. Due to the presence of the potential $V(z)$, only the momentum $p_x = \hbar k_x$ is conserved. We find the matrix elements of $\mathcal{H}$ in the basis of $\mathcal{H}_0$ indicated by $|k_x, n, \sigma\rangle$, with n the index of the sub-band and $\sigma = \pm 1$ for up or down spin, respectively. The SOI term contains terms $\sigma_z p_x$ and $-\sigma_x p_z$. For $\ell = n$, only the former term of $\mathcal{H}_{\mathrm{R}}$ is acting on the unperturbed states with the same spin state, so the matrix elements are

$$\langle k_x, \ell, \sigma|\mathcal{H}_{\mathrm{R}}|k_x, n, \sigma'\rangle = \frac{\hbar^2 k_{\mathrm{SO}} k_x}{m}\,\sigma'\delta_{\sigma,\sigma'}, \tag{15}$$

while, for $\ell \neq n$, the latter term $\mathcal{H}_{\rm R}$ couples sub-bands with opposite spin and parity, so the matrix elements are

$$\langle k_x, \ell, \sigma|\mathcal{H}_{\rm R}|k_x, n, \sigma'\rangle = J_{\ell,n}\delta_{\sigma,-\sigma'}, \tag{16}$$

with $J_{\ell,n}$ independent of the wavevector k_x:

$$J_{\ell,n} = \frac{{\rm i}\hbar^2 k_{\rm SO}}{m\,W}\frac{2\ell n}{\ell^2 - n^2}\left[1 - (-1)^{|\ell-n|}\right]. \tag{17}$$

If we express the energies in the unit $\hbar^2/2mW^2$, the lengths in W and the wavevectors in $1/W$, we recast the following matrix elements for the entire Hamiltonian $\mathcal{H}$:

$$\langle k_x, \ell, \sigma|\mathcal{H}|k_x, n, \sigma'\rangle = \left[\bar{E}_n^{(0)}(\bar{k}_x) + 2\bar{k}_{\rm SO}\bar{k}_x\sigma'\right]\delta_{\ell,n}\delta_{\sigma,\sigma'} + \bar{J}_{\ell,n}[1 - \delta_{\ell,n}]\delta_{\sigma,-\sigma'}, \tag{18}$$

where $\bar{k}_x = k_x W$, $\bar{E}_n^{(0)}(\bar{k}_x) = \bar{k}_x^2 + n^2\pi^2$, $\bar{k}_{\rm SO} = k_{\rm SO}W$, and $\bar{J}_{\ell,n}$ is proportional to the dimensionless SOI term $\bar{k}_{\rm SO}$

$$\bar{J}_{\ell,n} = {\rm i}\bar{k}_{\rm SO}\frac{4\ell n}{\ell^2 - n^2}\left[1 - (-1)^{|\ell-n|}\right]. \tag{19}$$

3.1. Perturbation theory

The correction to the unperturbed energies $\bar{E}_n^{(0)}$ within the first-order perturbation theory is simply derived by considering only the diagonal terms of equation (18). Therefore, to first order, the nth sub-band is simply affected by the spin slitting due to the contribution $\sigma_z p_x$ of $\mathcal{H}_{\rm SO}$:

$$\bar{E}_{n,\sigma}^{(1)}(\bar{k}_x) = \bar{E}_n^{(0)}(\bar{k}_x) + 2\bar{k}_{\rm SO}\bar{k}_x\sigma, \tag{20}$$

and eigenvectors equal to those of the unperturbed system. This splitting controlled by SOI gives rise to a first-order spectrum with crossings between sub-bands with opposite spins. For example, the first and second sub-bands intersect at $\bar{k}_x = \pm 3\pi^2/4\bar{k}_{\rm SO}$, and the others at larger values of $\bar{k}_x$. This suggests that the full effect of the interaction should remove this crossing by mixing the behaviour of coupled sub-bands. Due to the presence of those level crossings, the correction to the energy levels within the second-order perturbation theory fails for values of $\bar{k}_x$ close to intersections. Far from the crossing points, it is easy to derive the contribution to the second order to the energy:

$$\bar{E}_{n,\sigma}^{(2)} = \sum_{\ell(\neq n)}\sum_{\sigma'(\neq\sigma)}\frac{|\bar{J}_{\ell,n}|^2}{\pi^2(n^2 - \ell^2)} = -\bar{k}_{\rm SO}^2, \tag{21}$$

a quantity independent of k_x, n and σ. This result is indubitably valid for $\bar{k}_x = 0$. Indeed, it coincides with the result (13) obtained in the previous section by using the exact wavefunction. This shows that at $\bar{k}_x = 0$ the energy correction within the second-order perturbation theory is able to fully describe the energy spectrum. Also, the correction of the wavefunction at first order can be evaluated. If at zero order the spin is σ, at first order one takes the contribution from $-\sigma$:

$$\psi_{n,\sigma}^{(1)}(z) = \frac{\bar{k}_{\rm SO}}{4\pi^2}\sqrt{\frac{2}{W}}\left[S_{1,n}(z) - S_{2,n}(z)\right]|-\sigma\rangle, \tag{22}$$

with

$$S_{1,n}(z) = \Phi\left(e^{-2{\rm i}\pi z/L}, 2, \frac{-n}{2}\right) - \Phi\left(e^{-2{\rm i}\pi z/L}, 2, \frac{n}{2}\right), \tag{23}$$

and

$$S_{2,n}(z) = \Phi\left(e^{2{\rm i}\pi z/L}, 2, \frac{-n}{2}\right) - \Phi\left(e^{2{\rm i}\pi z/L}, 2, \frac{n}{2}\right), \tag{24}$$

where $\Phi(x, s, a) = \sum_{k=0}^{\infty} x^k/(a+k)^s$ is the Lerch transcendent function [19].

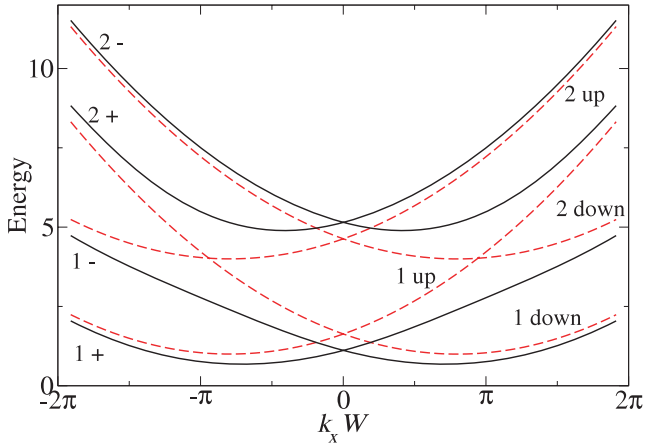

Figure 2. Energy levels of the two-band model (in units of $\hbar^2/2mW^2$) as a function of the dimensionless wavevector $k_x W$ for the value $k_{SO}W = \pi$ of the dimensionless spin–orbit parameter. The spectrum derived from the diagonalization of the two-band system, indicated in figure by 1+, 1−, 2+, and 2− (solid lines), is compared with that from first-order perturbation theory, indicated by 1 up, 1 down, 2 up, 2 down (dashed lines).

3.2. Two-band model

In order to investigate the effects of the coupling between sub-bands induced by SOI, it is convenient to analyse the two-band model that will be also considered in the section devoted to transport properties. This model takes only the first and the second sub-band of the unperturbed wire into account. The 4×4 problem can be decoupled into two 2×2 problems. The only thing to evaluate is $\bar{J}_{1,2} = -\mathrm{i}16\bar{k}_{SO}/3$. One gets 4 eigenvalues [13, 14]:

$$\epsilon_{1+}(\bar{k}_x) = \frac{5\pi^2}{2} + \bar{k}_x^2 - g_1(\bar{k}_x), \qquad \epsilon_{1-}(\bar{k}_x) = \epsilon_{1+}(-\bar{k}_x), \tag{25}$$

$$\epsilon_{2+}(\bar{k}_x) = \frac{5\pi^2}{2} + \bar{k}_x^2 - g_2(\bar{k}_x), \qquad \epsilon_{2-}(\bar{k}_x) = \epsilon_{2+}(-\bar{k}_x), \tag{26}$$

with

$$g_1(\bar{k}_x) = \frac{1}{2}\sqrt{(3\pi^2 - 4\bar{k}_x\bar{k}_{SO})^2 + \frac{1024\bar{k}_{SO}^2}{9}}, \qquad g_2(\bar{k}_x) = g_1(-\bar{k}_x). \tag{27}$$

The eigenvectors can also be calculated. For example, the eigenvector corresponding to ϵ_{1+} is

$$\psi_{1+}(x,z) = \mathrm{e}^{\mathrm{i}k_x x}\sqrt{\frac{2}{W}}\frac{1}{\sqrt{1+\left[f_1\left(\bar{k}_x\right)\right]^2}}\begin{pmatrix} \sin\left(\frac{\pi z}{W}\right) \\ \mathrm{i}f_1\left(\bar{k}_x\right)\sin\left(\frac{2\pi z}{W}\right) \end{pmatrix}, \tag{28}$$

with $f_1(\bar{k}_x)$ given by

$$f_1\left(\bar{k}_x\right) = \frac{3}{16\bar{k}_{SO}}\left[-\frac{3\pi^2}{2} + 2\bar{k}_{SO}\bar{k}_x + g_1(\bar{k}_x)\right]. \tag{29}$$

As shown in figure 2, the eigenvalues (solid lines) do not show any intersection for k_x different from zero. Therefore, the inter-band coupling removes the crossings of the first-order perturbation theory solution (dashed line). As a result, the energy eigenstates are no longer eigenstates of σ_z [14] and the spin state depends on the wavevector k_x. Close to the crossing point, the wavefunction of $1\uparrow$ and $2\downarrow$, for example, are strongly mixed in the mode

1+. However, far from the intersection, the mode given by the diagonalization preserves the original behaviour of the component wavefunctions. For example, if we analyse the behaviour of the eigenstate $\psi_{1+}(x, z)$, we get

$$\lim_{k_x \to -\infty} \psi_{1+}(x, z) = \psi_{1\uparrow}(x, z), \qquad \lim_{k_x \to \infty} \psi_{1+}(x, z) = \psi_{2\downarrow}(x, z). \tag{30}$$

The behaviour of the two-band model shows a general trend: by only taking into account the coupling between sub-bands the description is qualitatively correct. The crossing are artefacts of the lowest-order perturbation theory. The spectrum within the two-band model is reliable only for very narrow wires. In the general case, the low-energy description given by this model is too poor for the bands 2+ and 2−. This can be easily seen if one considers the energy values at $k_x = 0$. In fact one gets for sub-bands 1± and 2±, respectively, that the achieved values are

$$\epsilon_{1\pm} = \frac{5\pi^2}{2} - \frac{1}{2}\sqrt{9\pi^4 + \frac{1024\bar{k}_{\mathrm{SO}}^2}{9}}, \tag{31a}$$

$$\epsilon_{2\pm} = \frac{5\pi^2}{2} + \frac{1}{2}\sqrt{9\pi^4 + \frac{1024\bar{k}_{\mathrm{SO}}^2}{9}}. \tag{31b}$$

In the limit of small $\bar{k}_{\mathrm{SO}}$, they become

$$\epsilon_{1\pm} = \pi^2 - \frac{256}{27\pi^2}\bar{k}_{\mathrm{SO}}^2 \simeq \pi^2 - 0.961\bar{k}_{\mathrm{SO}}^2, \tag{32a}$$

$$\epsilon_{2\pm} = 4\pi^2 + \frac{256}{27\pi^2}\bar{k}_{\mathrm{SO}}^2 \simeq 4\pi^2 + 0.961\bar{k}_{\mathrm{SO}}^2. \tag{32b}$$

From the comparison with the exact solution we find that the lowest sub-bands acquire a correction with the right sign and very close to the exact result, while the upper sub-bands even have the wrong sign. Therefore, in order to give a reasonable description of the low-energy part of the spectrum, more bands are necessary. This will also play an important role in the transport properties.

3.3. Exact diagonalization

In order to verify the importance of including more than two sub-bands, one can directly diagonalize the Hamiltonian of the system [14]. This can be done by considering the matrix elements (18). In figure 3 we consider the diagonalization in the subspace of three spin-degenerate bands. It is apparent that already at this level the corrections to the level energies and wavefunctions are important for the second sub-band. For example, it is very close to the correct behaviour at $k_x = 0$. Considering l sub-bands for the diagonalization, one is able to get a reliable behaviour starting from sub-band 1 to $l - 1$.

4. Ballistic transport

In this section the issue is to study the quantum transport properties within the ballistic regime. The standard Landauer–Büttiker formalism will be employed. We will start by considering a wire divided into two different regions: one with SOI and one without. Then we take the case of a quantum wire with a finite SOI region into account. The results are obtained within the approximation of the two-band model and those results will be compared with a numerical tight-binding method.

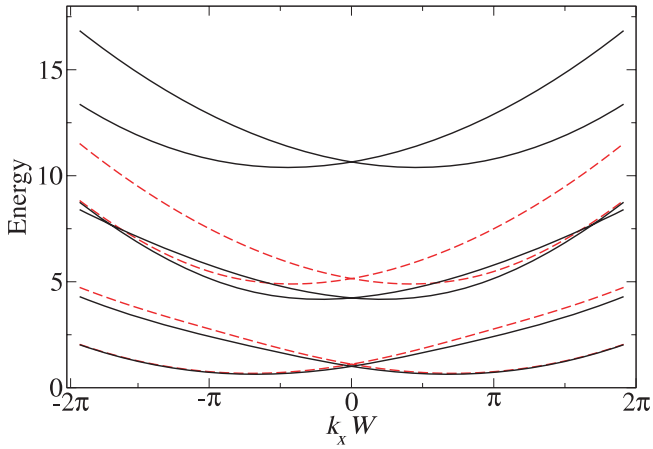

Figure 3. Energy levels of the wire (in units of $\hbar^2/2mW^2$) as a function of the dimensionless wavevector $k_x W$ for the value $k_{SO}W = \pi$ of the dimensionless spin–orbit parameter. The spectra derived from the diagonalization of the system with three sub-bands (solid line) and two sub-bands (dashed line) are shown.

4.1. Single interface

We consider a QW divided in two main regions: in the right region ($x > 0$) SOI is present while in the left region ($x < 0$) it is not. The interface separating the two regions is considered to be sharp and is described by a δ-like potential. The Hamiltonian of this hybrid system reads

$$\mathcal{H}_{\rm hyb} = \vec{p}\frac{1}{2m(x)}\vec{p} + V(z) + \frac{\hbar k_{\rm SO}(x)}{m_{\rm SO}}(\sigma_z p_x - \sigma_x p_z) - {\rm i}\sigma_z\frac{\hbar}{2m_{\rm SO}}\frac{\partial k_{\rm SO}(x)}{\partial x} + \frac{\hbar^2 u}{2m(x)}\delta(x). \tag{33}$$

We assume that the mass and the strength of the SOI are piecewise constant with $k_{\rm SO}(x) = k_{\rm SO}\theta(x)$. For simplicity the mass is considered equal on both sides of the interface. The fourth term is necessary to get $\mathcal{H}_{\rm hyb}$ Hermitian. At the interface the spinor eigenstates of $\mathcal{H}_{\rm hyb}$ have to be continuous, whereas their derivatives have a discontinuity $u - {\rm i}\sigma_z k_{\rm SO}$ due to the SOI and to the δ-like potential in $x = 0$:

$$\psi(0^+) = \psi(0^-), \tag{34a}$$

$$\left.\frac{\partial\psi(x)}{\partial x}\right|_{x=0^+} - \left.\frac{\partial\psi(x)}{\partial x}\right|_{x=0^-} = (u - {\rm i}\sigma_z k_{\rm SO})\psi(0). \tag{34b}$$

In order to study the effects of the sub-band hybridization on the transport properties, we start by considering the injection of carriers only within the first sub-band. This can be achieved by requiring that the second sub-band is behaving as an evanescent wave. In this context the equations (34*a*) and (34*b*) are reduced to a set of two decoupled systems of four times four equations for the variables r_{1+}, t_{1+}, r_{2-}, t_{2-} and r_{1-}, t_{1-}, r_{2+}, t_{2+} respectively, where $t_{1(2),+(-)}$ and $r_{1(2),+(-)}$ are the transmission and the reflection amplitudes in the first (second) sub-band with spinor $+$ $(-)$ respectively. The knowledge of the transmission and reflection amplitudes permits us to evaluate the probability current and, as a consequence, the transmission probabilities for spin-up and spin-down carriers. Due to the presence of SOI only for $x > 0$, the probability current has two different forms, given by

$$\vec{j} = \frac{1}{m}\begin{cases}{\rm Re}\left\{\psi^\dagger\vec{p}\,\psi\right\} & \text{for } x < 0\\ {\rm Re}\left\{\psi^\dagger\left[\vec{p} + \hbar k_{\rm SO}\left(\hat{y}\times\vec{\sigma}\right)\right]\psi\right\} & \text{for } x > 0\end{cases} \tag{35}$$

where ψ is the wavefunction solution of the system of equations (34*a*) and (34*b*). A direct evaluation of the transmission probabilities [20] results in the following expressions:

$$T_\uparrow = \frac{|t_{1+}|^2}{k_{\rm in}}\left[k_{1+}(k_{\rm in}) + k_{\rm SO}\langle\sigma_z\rangle_{1+}\right], \tag{36a}$$

$$T_\downarrow = \frac{|t_{1-}|^2}{k_{\rm in}}\left[k_{1-}(k_{\rm in}) + k_{\rm SO}\langle\sigma_z\rangle_{1-}\right], \tag{36b}$$

where $k_{\rm in}$ is the injection momentum and $k_{1+}(k_{\rm in})$ and $k_{1-}(k_{\rm in})$ are the momentum relative to $k_{\rm in}$ for the two spin-resolved sub-bands. The factors $\langle\sigma_z\rangle_{1+}$ and $\langle\sigma_z\rangle_{1-}$ are the expectation values of σ_z on the two spin-resolved sub-band wavefunctions and are defined as

$$\langle\sigma_z\rangle_{1\pm} = \pm\frac{1 - f_1(\pm k_{1\pm})^2}{1 + f_1(\pm k_{1\pm})^2} \tag{37}$$

where the function f_1 has been provided with equation (29). Because of the absence of SOI for $x < 0$, the reflection probabilities are simply defined as $R_\uparrow = |r_{1+}|^2$ and $R_\downarrow = |r_{1-}|^2$. The system Hamiltonian $\mathcal{H}_{\rm hyb}$ is invariant under time-reversal symmetry and, as a consequence, the following relations hold: $R_\uparrow = R_\downarrow$ and $T_\uparrow = T_\downarrow$. This means that spin-up and spin-down carriers are transmitted through the interface in the same way.

We consider the injection of a spin-unpolarized mixture of carriers with injection momentum $k_{\rm in}$. In terms of density matrix we have

$$\rho_{\rm in} = \tfrac{1}{2}|\uparrow\rangle\langle\uparrow| + \tfrac{1}{2}|\downarrow\rangle\langle\downarrow| \tag{38}$$

with the property that $\langle\sigma_z\rangle_{\rm in} = {\rm Tr}\{\rho_{\rm in}\sigma_z\} = 0$. The density matrix of the transmitted carriers is expressed by the relation

$$\begin{aligned}\rho_{\rm out} &= \frac{T_\uparrow}{T_\uparrow + T_\downarrow}|1+\rangle\langle 1+| + \frac{T_\downarrow}{T_\uparrow + T_\downarrow}|1-\rangle\langle 1-| \\ &= \tfrac{1}{2}|1+\rangle\langle 1+| + \tfrac{1}{2}|1-\rangle\langle 1-|\end{aligned} \tag{39}$$

where $|1\pm\rangle$ are the wavefunctions of the spin-resolved sub-bands. We can now evaluate the polarization of the output carriers; this is expressed by

$$\begin{aligned}\langle\sigma_z\rangle_{\rm out} &= \tfrac{1}{2}\langle\sigma_z\rangle_{1+} + \tfrac{1}{2}\langle\sigma_z\rangle_{1-} \\ &= \frac{1}{2}\left(\frac{1 - f_1(k_{1+})^2}{1 + f_1(k_{1+})^2} - \frac{1 - f_1(-k_{1-})^2}{1 + f_1(-k_{1-})^2}\right).\end{aligned} \tag{40}$$

Figure 4 shows the polarization (40) as a function of the injection energy for various values of the SOI. The injection energy is limited within the first two spin-resolved sub-bands. It is clear that when the SOI is zero (dotted line) there is no polarization, but as soon as the SOI is different from zero, the polarization gets a finite value, which increases as a function of SOI for a fixed energy. Those results are in accordance with Governale and Zülicke [14], who showed a negative polarization for carriers in the first two spin-resolved sub-bands and positive injection energies.

4.2. Wire with finite SOI region

We consider a QW composed of three parts: two external regions ($x < 0$ and $x > L$) without SOI, and a central one ($0 < x < L$) where SOI is present. We consider the hybrid system Hamiltonian of equation (33), with $k_{\rm SO}(x) = k_{\rm SO}\theta(x)\theta(L - x)$ and two δ-like potentials of $x = 0$ and L. Also in this case, for simplicity, the mass is assumed constant along the wire.

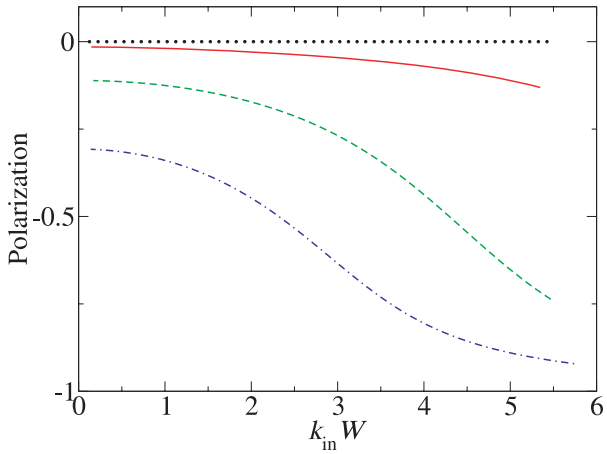

Figure 4. Polarization (40) as a function of the injection energy for $\bar{k}_{SO} = 0$ (dotted line), $\bar{k}_{SO} = 1$ (solid line), $\bar{k}_{SO} = 2$ (dashed line) and $\bar{k}_{SO} = 3$ (dotted–dashed line).

As for the single interface case, the spinor eigenstates of H_{hyb} are continuous at the interfaces, whereas their derivatives have discontinuities in $x = 0$ and L:

$$\psi(0^+) = \psi(0^-), \tag{41a}$$

$$\left.\frac{\partial\psi(x)}{\partial x}\right|_{x=0^+} - \left.\frac{\partial\psi(x)}{\partial x}\right|_{x=0^-} = (u - \mathrm{i}\sigma_z k_{SO})\psi(0), \tag{41b}$$

$$\psi(L^+) = \psi(L^-), \tag{41c}$$

$$\left.\frac{\partial\psi(x)}{\partial x}\right|_{x=L^+} - \left.\frac{\partial\psi(x)}{\partial x}\right|_{x=L^-} = (u + \mathrm{i}\sigma_z k_{SO})\psi(L). \tag{41d}$$

As a first step, we consider carriers with injection energy within the first two spin-resolved sub-bands and with evanescent waves for the following two. The equations (41*a*)–(41*d*) reduce to a set of two decoupled system of equations, with relevant terms t_{R1+}, t_{R1-}, r_{L1+} and r_{L1-}. Those are practical for evaluating the transmission and the reflection probabilities for spin-up and spin-down carriers. As expected, because of the absence of SOI in the external regions we get

$$T_\uparrow = |t_{R1+}|^2, \qquad T_\downarrow = |t_{R1-}|^2, \tag{42a}$$

$$R_\uparrow = |r_{L1+}|^2, \qquad R_\downarrow = |r_{L1-}|^2. \tag{42b}$$

Due to time-reversal symmetry, it results that the value of the transmission probability $T_\uparrow$ for incoming spin-up carriers is equal to $T_\downarrow$ for incoming spin-down carriers. It is relevant to study transport properties when an unpolarized mixture of spin-up and spin-down carriers is injected into the system. The incoming and the outgoing density matrices are described by the expressions (38) and (39) respectively, where now the states $|1\pm\rangle$ are the output wavefunctions in the second region without SOI. As in the previous section, we can evaluate the polarization as the average value of the σ_z operator, and obtain as a result

$$\langle\sigma_z\rangle_{out} = T_\uparrow - T_\downarrow = 0. \tag{43}$$

The effect of spin polarization due to the first interface is completely cancelled by the second one; therefore it is not possible to observe any spin polarization [14]. This result can also be derived by a symmetry consideration: let us consider the scattering matrix $\mathcal{S}_{QW}$ of the

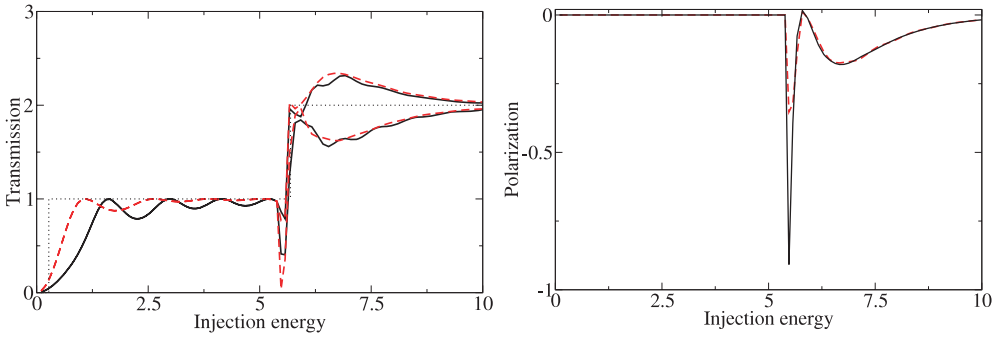

Figure 5. Left panel: spin-resolved transmissions as a function of the injection energy and for two different values of the transparency of the barriers: $u = 1.0$ (solid lines) and $u = 0.1$ (dashed lines). The dotted line indicates the opening of the sub-bands in the absence of SOI. The dimensionless SOI is $\bar{k}_{\mathrm{SO}} = 1.4$ and the central region is $L = 3W$. Right panel: spin polarization $\langle\sigma_z\rangle$ as a function of the injection energy and for two different value of the δ-barrier transparency. The same parameters as in the left panel are used.

QW. In the absence of a magnetic field time-reversal symmetry is preserved; therefore, as a consequence, for $\mathcal{S}_{\mathrm{QW}}$ the following important relation holds:

$$\mathcal{S}_{\mathrm{QW}} = \Sigma_y \mathcal{S}_{\mathrm{QW}}^{\dagger} \Sigma_y \tag{44}$$

where $\Sigma_y = \begin{pmatrix} \sigma_y & 0_2 \\ 0_2 & \sigma_y \end{pmatrix}$. It is clear for equation (44) that in the case of only one conducting channel the spin-flip transmission terms must be zero, and as a consequence the polarization is absent [15].

As a further step, we study the transport properties when carriers are injected also within the second two spin-resolved sub-bands. In this limit all the evanescent modes are transformed into conducting ones. Using equations (38) and (39) for the incoming and the outgoing density matrix, the polarization is expressed by

$$\langle\sigma_z\rangle_{\mathrm{out}} = \frac{1}{2}\left(\frac{T_{1+}(0) + T_{2+}(0) - T_{1-}(0) - T_{2-}(0)}{T_{1+}(0) + T_{2+}(0) + T_{1-}(0) + T_{2-}(0)} + \frac{T_{1+}(\pi/2) + T_{2+}(\pi/2) - T_{1-}(\pi/2) - T_{2-}(\pi/2)}{T_{1+}(\pi/2) + T_{2+}(\pi/2) + T_{1-}(\pi/2) + T_{2-}(\pi/2)}\right), \tag{45}$$

where 0 and $\pi/2$ denote incoming up- and down-carriers respectively.

In figure 5 (left panel) we show the spin-resolved transmissions as a function of the injection energy below and above the bottom of the second two sub-bands and for two values of the transparency u of the interfaces (strength of the δ-function potential in equation (33)). The behaviour below the threshold clearly shows Fabry–Perot oscillations due to multiple reflection effects within the central region; moreover, the strength of those oscillations is decreasing for increasing transparency of the two δ-barriers. A second important feature of the behaviour is that, up to the threshold, owing to the time-reversal symmetry, the two spin-resolved components possess the same value. When the injection energy crosses the bottom of the second two sub-bands, a new behaviour appears. The two spin-resolved transmissions take different values: the difference between those two is bigger near to the sub-band threshold and is decreasing with increasing energy. This can be well understood if we relate this phenomenon to the sub-band hybridization. As shown in figures 2 and 3, the SOI strongly modifies the parabolic-like behaviour of the spin-resolved sub-bands when new sub-bands are opening, and

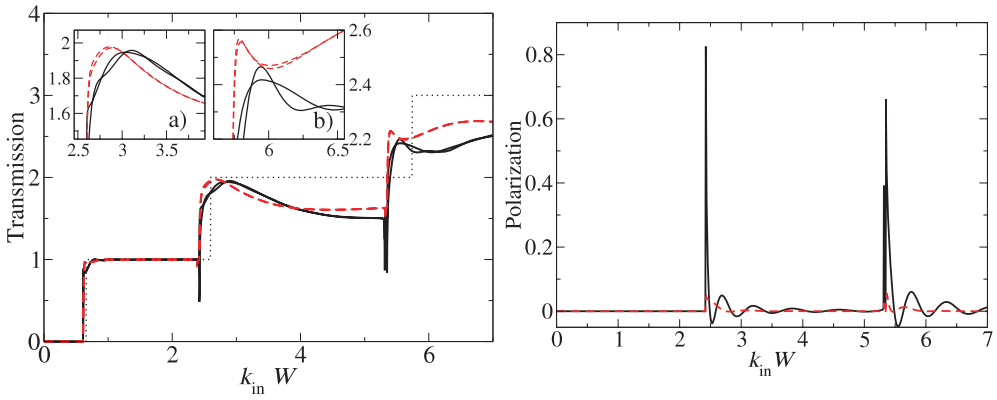

Figure 6. Left panel: numerical spin-resolved transmissions as a function of the injection energy and for two different values of the switching region of SOI: $L_{sr}W^{-1} \sim 0.07$ (solid lines) and $L_{sr}W^{-1} \sim 0.7$ (dashed lines). The dotted line indicates the opening of the sub-bands in the absence of SOI. The dimensionless SOI is $\bar{k}_{SO} = 1.4$ and the central region is $L = 3W + 2L_{sr}$. In the insets (a) and (b) are shown the magnification for the steps relative to the opening of the second and the third sub-band, respectively. Right panel: spin polarization $\langle\sigma_z\rangle$ as a function of the injection of energy and for the two different values of $L_{sr}W^{-1}$. The same parameters as in the left panel are used.

this effect vanishes at higher energies. In contrast to the results of Governale and Zülicke [14], figure 5 clearly shows how polarization effects can manifest themselves when the second two spin-resolved sub-bands are also involved in the transmission mechanism. This is more clear in figure 5 (right panel), where the polarization is shown as a function of the injection energy. The polarization is zero below the bottom of the second two sub-bands and has oscillating behaviour above it. This particular shape of the polarization can also be understood in terms of the formation of spin-dependent bound states at energies closer to the opening of the second two sub-bands. Those bound-state oscillations are clearly visible in the polarization pattern, and it is evident how they are enhanced when the δ-barrier transparency is decreased.

The effects on spin transport due to higher sub-bands can be numerically verified. For this purpose we employ a tight-binding model of the Hamiltonian (1); the spin-dependent scattering coefficients are obtained by projecting the corresponding spin-dependent Green function of the open system onto an appropriate set of asymptotic spinors defining incoming and outgoing channels. A real-space discretization of the Schrödinger equation in combination with a recursive algorithm for the computation of the corresponding Green function has been implemented [20]. This formalism allows a convenient treatment of different geometries as well as different sources of scattering within the same framework [21].

The δ-barriers are introduced in the tight-binding calculation by dividing the central region into three parts in order to modulate the switching region L_{sr} for the SOI. A long switching region will correspond to a high transparency, and vice versa. In figure 6 (left panel) we show the spin-resolved transmission as a function of the injection energy and for two different lengths of the switching region. The system parameters are chosen in order to have three active sub-bands in the case of injection within the highest energy allowed by the tight-binding approximation of the Hamiltonian (1). Injecting carriers within the first two spin-resolved sub-bands reproduces the result from time-reversal symmetry: spin-up and spin-down transmissions coincide. As soon as the second two sub-bands are opened we can observe a difference in their values. This difference tends to decrease for increasing energy but is, then, enhanced by the

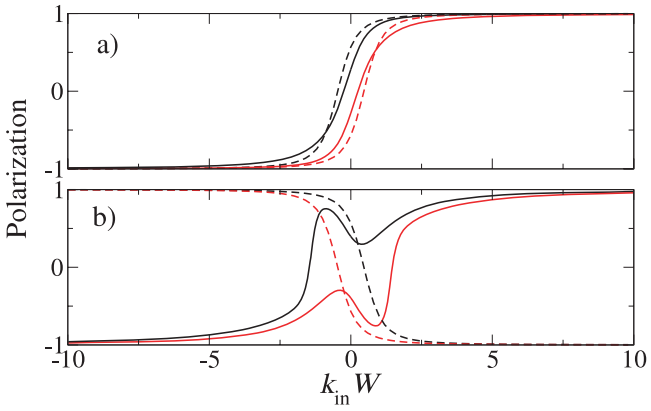

Figure 7. Polarization as a function of the injection energy for the two-band (dashed line) and the N-band (solid line) models, respectively. Panel (a) first sub-band, panel (b) second sub-band. For both the panels $N = 50$.

opening of the third two sub-bands[5]. This is clear from figure 6 (right panel), where we show the polarization as a function of the injection energy. Here it is also possible to observe how the strength of the polarization oscillations is strongly reduced by changing the length of the switching region.

The polarizations at the opening of the second two spin-resolved sub-bands in the case of the two-band model (figure 5) and for the numerical tight-binding method (figure 6) show an opposite value. This can be well understood if we consider the polarization within the first and the second sub-band for an infinite long wire in the two-band and in the N-band models, respectively. In figure 7, we show the polarization for the first sub-band (upper panel); it is evident that there is a small deviation of the two-band model (dashed lines) from the N-band model. But this deviation is stronger for the second sub-band (lower panel), resulting in a completely opposite value at large energies. This well reveals how the two-band model can only qualitatively reproduce the exact calculation, but fails in the quantitative estimation.

5. Conclusions

We have studied the properties of a QW in the presence of Rashba SOI. The spectral properties have been investigated both from the point of view of the exact wavefunctions and within the second-order perturbation theory approach. Furthermore, a numerical diagonalization procedure has been implemented in order to study the spectral properties for the system in the presence of N sub-bands. We have used this last method with two sub-bands within the so-called two-band model. We have shown that this is a good description for the full properties of the first sub-band but not of the second one. This model has also been used in order to study the transport properties of a system with an interface between a region with and without SOI. We have shown that the interface is spin selective and that the crossing of unpolarized carriers through the interface can give rise to a non-zero polarization. We have studied spin transport also by injecting carriers within the first and the second sub-band. We have shown that at the opening of each new channel the sub-band hybridization can give rise to spin-selective

[5] Bound states owing to Fano resonances in a quantum wire with Rashba spin–orbit interaction have also been recently investigated by Sánchez and Serra [22].

bound states reflecting in a oscillating spin polarization. Those results have been confirmed by numerical calculation obtained within the tight-binding approximation.

Acknowledgments

We acknowledge I Adagideli, M Scheid and M Strehl for useful discussions. DB is grateful for the hospitality at the Max-Planck-Institut für Physik komplexer Systeme (Dresden), where this paper was partially written, and for the financial support of Deutsche Forschungsgemeinschaft within the cooperative research centre SFB 689 'Spin phenomena in low dimensions'.

References

[1] Žutíc I, Fabian J and Sarma S D 2004 *Rev. Mod. Phys.* **76** 323
[2] Wolf S A *et al* 2001 *Science* **294** 1488
[3] Datta S and Das B 1990 *Appl. Phys. Lett.* **56** 665
[4] Schmidt G *et al* 2000 *Phys. Rev.* B **62** 2790
[5] Jedema F J, Fillip A T and van Wess B J 2001 *Nature* **410** 345
[6] Valenzuela S O and Tinkham M 2006 *Nature* **442** 176
[7] Dresselhaus G 1955 *Phys. Rev.* **100** 580
[8] Rashba E 1960 *Fiz. Tverd. Tela (Leningrad)* **2** 1224
Rashba E 1960 *Sov. Phys.—Solid State* **2** 1109 (Engl. Transl.)
[9] Nitta J, Akazaki T, Takayanagi H and Enoki T 1997 *Phys. Rev. Lett.* **78** 1335
[10] Schäpers Th, Engels J, Klocke T, Hollfelder M and Lüth H 1998 *J. Appl. Phys.* **83** 4324
[11] Grundler D 2000 *Phys. Rev. Lett.* **84** 6074
[12] Schäpers Th, Knobbe J and Guzenko V A 2004 *Phys. Rev.* B **69** 235323
[13] Mireles F and Kirczenow G 2001 *Phys. Rev.* B **64** 024426
[14] Governale M and Zülicke U 2002 *Phys. Rev.* B **66** 073311
[15] Zhai F and Xu H Q 2005 *Phys. Rev. Lett.* **94** 246601
[16] Ramaglia V M, Bercioux D, Cataudella V, De Filippis G, Perroni C A and Ventriglia F 2003 *Eur. Phys. J.* B **36** 365
[17] Ramaglia V M, Bercioux D, Cataudella V, De Filippis G and Perroni C A 2004 *J. Phys.: Condens. Matter* **16** 9143
[18] Bercioux D and Ramaglia V M 2005 *Superlatt. Microstruct.* **37** 337
[19] Laurincikas A and Garunkstis R 2003 *The Lerch Zeta-Function* (Dordrecht: Kluwer–Academic)
[20] Ferry D K and Goodnick S M 1997 *Transport in Nanostructures* (Cambridge: Cambridge University Press)
[21] Frustaglia D, Hentschel M and Richter K 2004 *Phys. Rev.* B **69** 155327
[22] Sánchez D and Serra L 2006 *Phys. Rev.* B **74** 153313